Spin Counting in Dipolar Coupled Spin 1/2 Systems by Multiple Quantum Coherence

Son-Jong Hwang and B. C. Gerstein

Department of Chemistry and Ames Laboratory
Iowa State University, Ames, Iowa 50011

Contents

I. Introduction

The aim of this review is to present, in an easily understandable manner, and perhaps with a fresh perspective, the ideas behind the creation and detection of multiple quantum coherence in ensembles of homonuclear dipolar coupled spin 1/2 systems. To this end, both theoretical ideas and experimental details will be presented such that readers will have the background to perform such experiments on their own instruments, given the appropriate phase shifting capabilities.

With the exception of the results given in Section VII on one use of multiple quantum coherence in counting numbers of coupled protons in C_mH_m fragments on catalysts, the authors make no claim to originality in the concepts and results presented here. For example, the development of multiple quantum coherence among coupled protons in the liquid crystal p-hexyl-p'-cyano biphenyl in the nematic phase which we show for a single quantum propagator in Figure 15 (*vide infra*) was first presented in 1986 by Baum and Pines using a double quantum propagator. A similar remark applies to the results shown in Figure 13.

Spin counting by multiple quantum coherence is one of a variety of possible two dimensional NMR experiments which first began to appear in the mid 1970's (1–3) and have since been extensively reviewed (4–8).

In the specific case of using MQ coherence to enumerate numbers of strongly coupled spins in ensembles of coupled clusters of protons in solids (9, 10) the initial work developed multiple quantum coherence in steps of two quanta, such that values of multiple quantum coherence, k, of 0, 2, 4, 6..., or 1, 3, 5, ... might be detected. Later work (*vide infra*) resulted in the use of pulse sequences which developed multiple quantum coherence in steps of one quantum, such that values of k = 0, 1, 2, ...

could be detected.

In liquids, the coupling mechanism used to produce multiple quantum coherence is the two-body scalar, or J-coupling. The secular portion of the spin-space part of this interaction is $I_z S_z$ for the heteronuclear case. In solids, the case to be discussed here, the interaction is the two-body homonuclear dipolar coupling between spin 1/2 systems, e.g. among protons is a solid. The secular portion of the spin-space part of this interaction is $\mathbf{I}_1 \bullet \mathbf{I}_2 - 3I_{z1} I_{z2}$. The pulse sequences used to develop multiple quantum coherence in the latter case will therefore differ from those used for the former, in the same sense that the dipolar echo sequence, (τ, 90_x, τ, 90_y, τ) differs from the spin echo sequence (τ, 180_x, τ). However, the extension of the present description to heteronuclear dipolar coupling, and to scalar coupling will hopefully be obvious, with the techniques used to generate, and detect multiple quantum coherence being more easily achieved than in the present case.

II. Single-Quantum Coherence

We first ask "what do we observe in an NMR experiment?" The answer is always a transverse component of spin angular momentum. With phase detection along y in the rotating frame, what is observed is

$$\text{FID} \sim < I_y(t) > = \text{Tr}\{\rho(t) I_y\} \qquad (1)$$

From this formalism it is immediately obvious that we are invoking the use of the quantum statistical method, in that the density operator, ρ, ***must*** be used to describe the phenomena discussed here (11).

The FID, the time dependence of which is given by $\rho(t)$, and the phase of which is specified in this case by the operator I_y, is driven by the presence of time-independent Hamiltonians, $\hat{H}$, as follows:

$$\rho(t) = \exp - \{i\hat{H}t\} \cdot \rho(0) \cdot \exp\{i\hat{H}t\} \qquad (2)$$

The spectrum is obtained by Fourier transformation of the FID. We remind ourselves of the quantum mechanics involved in this statement with a short review.

We consider an ensemble of identical systems, each described by a set of stationary states. These identical systems for purposes of the present discussion might be "isolated" nuclear spins (e.g. ^{13}C nuclei at a natural abundance of 1.1% decoupled from other nuclei via strong rf decoupling), or isolated pairs of nuclear spins (e.g. pairs of protons in partially hydrated calcium sulfate, $CaSO_4.xH_2O$, with $x < 2$), or many ($\sim 10^{23}$) protons in strongly dipolar coupled solids. The nuclear spin basis functions appropriate to describe the systems of the ensemble will therefore in general be many-body stationary states which we label $|M_s>$. These are eigenstates of the total z component of nuclear spin angular momentum such that

$$I_z|M_a> = s|M_a> \qquad (3a)$$

Two of these many body states, $|M_a>$, $|M_b>$, differ by $k = a - b$ in z component of total angular momentum. Further, the state of each system can in general be a time-dependent superposition of these stationary states:

$$|\Psi(t)> = \sum_j c_j(t)|M_j> \qquad (3b)$$

For example, in ensembles which consist of coupled pairs of spin 1/2 nuclei, where the coupling interaction is small compared to the Zeeman interaction, the stationary states of the coupled systems can be arranged to be eigenfunctions of the square of the total spin operator, I^2, and of the z component of spin I_z. Two coupled spins can have maximum total spin $I = 1$, and z component $-I \leq I_z \leq I$ in steps of unity. Three coupled spins can have maximum total spin $I = 3/2$, etc. It is these many-spin states which are designated as $|M_a>$ above.

We remember that the probability of finding any system in stationary state $|M_s>$ is

$$P_s = \overline{c_s^*(t)c_s(t)} = \overline{c_s(t)c_s^*(t)}, \qquad (4)$$

where the bars above the c_s's mean an ensemble average. The operator ρ is defined by the ensemble average of the product

$$\rho = |\Psi >< \Psi| \qquad (5)$$

such that the i,jth matrix element is

$$\rho_{ij} = \overline{< i|\Psi >< \Psi|j >} = \overline{c_i c_j^*} \qquad (6)$$

A non-vanishing value of ρ_{ss} therefore represents a population of the state $|M_s>$. An observable signal in NMR means a non-vanishing value of $\rho_{s,s+1}$. This means that in the ensemble of systems being observed, there is a phase coherence in the ensemble associated with system states $|M_s>$ and $|M_{s\pm1}>$. We designate this a ***single quantum coherence***. This is to say that we observe a decaying oscillation resulting from a coherence of the ensemble in which the time-dependent state responsible for the behavior of the system is a superposition of two states differing from each other by a single quantum. The most familiar example is the case of an ensemble of single spin 1/2 systems, in which case the two basis states are $|M_r> \equiv |\alpha> \equiv |1/2>$, and $|M_{r-1}> = |M_s> = |\beta> \equiv |-1/2>$. A non-vanishing component of transverse angular momentum is represented by a coherence in the ensemble of systems with a superposition of states consisting of two stationary states which differ from each other by 1 in expectation value of I_z;

$$|\Psi> = c_{1/2}(t)|\alpha> + c_{-1/2}(t)|\beta> \equiv c_\alpha|\alpha> + c_\beta|\beta> \tag{7}$$

such that the ensemble average of the product $c_\alpha(t)c^*_\beta(t)$ is non-zero. For example, such would be the case immediately after a 90°_x pulse, with rf field intensity ω_1/γ, and the values of the c_k's would be

$$\begin{gathered} c_\alpha(t = \pi/2\omega_1) = 1/\sqrt{2} \\ \text{and} \\ c_\beta(t = \pi/2\omega_1) = i/\sqrt{2} \end{gathered} \tag{8}$$

In this case, one calculates that the expectation values of I_x and I_z are zero, and 1/2 for I_y.

Statistical thermodynamics enters when we consider that the ensemble in question is prepared in some equilibrium state before observation, i.e. we expose an ensemble of nuclear spins, **I**, in a field until equilibrium is achieved under the Zeeman interaction $\hat{H}_z$, and

$$\rho(0) \equiv \rho_{eq} = (1/Z)\exp - \{\hat{H}_z/k_BT\} \sim \sum_i I_{zi}, \qquad i = 1, 2, \ldots \tag{9}$$

is the operator form of ρ. Z is the ensemble partition function.

III. Coherent Averaging

We next remind ourselves of the results of coherent averaging theory as applied to the spin portion of internal Hamiltonians (12). We first note that nuclear spin Hamiltonians may in general be expressed as a product of a constant characteristic of the interaction in question, and of "spin space" operators. For example, for the heteronuclear dipolar interaction between spins **I** and **S**, the constant is $(\gamma_I\gamma_S/r^3_{IS})$, the "real space" portion is $(1\text{–}3\cos^2\theta)$, and the "spin space" portion is I_zS_z. It is assumed that the real-space portion of the internal Hamiltonians are constant in the experiments under consideration, i.e. there is no molecular motion or experimenter-supplied sample spinning.

When we manipulate $\hat{H}_{int}$ by rf pulse sequences which are cyclic (the ensemble is returned to its initial state after a cycle of rf pulses, meaning that the propagator $U_{rf}(t_c,0)$ associated with the pulse train from time zero to time t_c, is unity at cycle times t_c, and integer multiples of these times) and periodic, the leading term in the result, observed at cycle times nt_c is

$$\rho(nt_c) = \exp\{-i\bar{H}^{(0)}nt_c\} \cdot \rho(0) \cdot \exp\{i\bar{H}^{(0)}nt_c\} \tag{10}$$

where $\bar{H}^{(0)}$ is the time average of a static internal Hamiltonian made time dependent by the rf pulses.

$$\bar{H}^{(0)}_{int} = (1/t_c)\int_o^{t_c} dt\tilde{H}_{int}(t) \tag{11}$$

$\tilde{H}_{int}(t)$ is the instantaneous value of the internal Hamiltonian as determined by the rf pulses:

$$\tilde{H}_{int}(t) = U^{-1}_{rf}(t,0)H_{int}U_{rf}(t,0) \tag{12}$$

$U_{rf}(t,0)$ is the propagation operator due to the rf pulses from time zero to time t. For n time intervals δ_1, followed by δ_2, followed by $\ldots\delta_n$, U_{rf} may be expressed as the product

$$U_{rf}(t,0) = U_{rf}(\delta_n)\ldots U_{rf}(\delta_1) \tag{13}$$

whereby

$$U^{-1}_{rf}(t,0) = U^{-1}_{rf}(\delta_1)\ldots U^{-1}_{rf}(\delta_n) \tag{14}$$

Eq. (12) can always be expressed as a product of rotations in spin space acting on components of angular momentum operators. For example, if the rf

pulse sequence (τ, 180_y, τ) with perfect δ function rf pulses produces U_{rf}, then at times $0 \leq t \leq \tau$, when the rf Hamiltonian is zero, U_{rf} (t,0) takes the form $e^0 = 1$, and in this time interval, $\tilde{I}_z = e^0 I_z e^0 = 1 \cdot I_z \cdot 1$ which we may formally identify as a rotation, R, of unity, performed on I_z, symbolized by $RI_z = 1 \cdot I_z$. At time $t = \tau$, the rf Hamiltonian corresponds to an infinitely sharp 180° rotation about the y axis. $U_{rf}(t = \tau) = e^{i\pi I}y$, and the physical result is a 180_y rotation, R_{180y}. For $\tau < t \leq 2\tau$, the rf again is zero, and U_{rf} is unity. Under this sequence, therefore, with the spin portion of H_{int} being proportional to I_z, keeping in mind the time ordering dictated by equations (12) and (14), we find

$$\begin{aligned} 0 \leq t < \tau, \tilde{I}_z &= 1 \cdot I_z = I_z \\ t = \tau, \tilde{I}_z &= 1 \cdot R_{180y} I_z = -I_z \\ \tau < t \leq 2\tau, \tilde{I}_z &= 1 \cdot R_{180y} \cdot 1 \cdot I_z = -I_z \end{aligned} \tag{15}$$

The familiar result is that ***at cycle times*** $2n\tau$, under the spin-echo sequence $(\tau, 180, \tau)^n$, chemical shifts and field inhomogeneities, with spin operators I_{zk}, vanish (but other interactions, such as homonuclear dipolar coupling, do not). This is to say that at cycle times $2n\tau$, with the internal Hamiltonian being proportional to I_z, that $\bar{H}^{(0)}_{int}$ is zero; i.e.

$$\bar{H}^{(0)}_{cs} \sim \int_0^{2n\tau} dt U^{-1}_{rf}(t) \tilde{H}_{cs} U_{rf}(t) = \omega_{cs}[I_z\tau + (-I_z)\tau] = 0 \tag{16}$$

where ω_{cs} is a product of a constant and the real-space portion of the chemical shift Hamiltonian.

Another perhaps less familiar result is that under symmetry adapted dipolar decoupling sequences $[\tau, 90_x, \tau, 90_y, \tau]$, homonuclear dipolar terms vanish, but chemical shifts are scaled. Consider the WAHUHA symmetry adapted version of the above dipolar echo sequence, which is $[\tau, 90_x, \tau, 90_y, 2\tau, 90_{\bar{y}}, \tau, 90_{\bar{x}}, \tau]$. Using equations (12)–(14), we find for ideal δ function rf pulses, the following values of $\tilde{I}_z(t)$:

$$\begin{aligned} 0 \leq t < \tau; \tilde{I}_z &= 1 \cdot I_z = I_z \\ t = \tau; \tilde{I}_z &\Rightarrow 1 \cdot R_{90\bar{x}} I_z = -I_y \\ \tau < t < 2\tau; \tilde{I}_z &= 1 \cdot R_{90\bar{x}} \cdot 1 I_z = -I_y \\ t = 2\tau; \tilde{I}_z &\Rightarrow 1 \cdot R_{90\bar{x}} \cdot 1 \cdot R_{90\bar{y}} I_z = -I_x \end{aligned} \tag{17a}$$

etc., from which we may immediately infer that, the scalar product $\mathbf{I_1 \bullet I_2}$ being invariant to rotation, the time dependence of the operator $H_{zz} = (\mathbf{I_1 \bullet I_2} - 3I_{z1}I_{z2})$ is as follows:

$$\begin{aligned} 0 \leq t < \tau;\ \tilde{H}_{zz} &= H_{zz} \\ t = \tau; I_{z1}I_{z2} &\Rightarrow I_{y1}I_{y2} \text{ so } \tilde{H}_{zz} \Rightarrow H_{yy} \end{aligned} \tag{17b}$$

etc. Then the two-body average homonuclear dipolar Hamiltonian is

$$\begin{aligned} \bar{H}^{(0)}_{DII} = (\omega_D/6\tau)[&\tau\{I_1 \cdot I_2 - 3I_{z1}I_{z2}\} + \tau\{I_1 \cdot I_2 - 3I_{y1}I_{y2}\} \\ &+2\tau\{I_1 \cdot I_2 - 3I_{x1}I_{x2}\} + \tau\{I_1 \cdot I_2 - 3I_{y1}I_{y2}\} \\ &+\tau\{I_1 I_2 - 3I_{z1}I_{z2}\}] \\ &\equiv \omega_D[H_{zz} + H_{yy} + H_{xx}]/3 = 0 \end{aligned} \tag{18}$$

where ω_D is a product of a constant and the real-space portion of the space-spin product dipolar Hamiltonian.

An important result just seen is that the sum

$$[H_{xx} + H_{yy} + H_{zz}]\tau = \sum H_{kk} = 0 \tag{19}$$

for two spins I_1 and I_2. ***In both of the above cases***, the average Hamiltonian for a specific interaction is made to vanish, leaving remaining interactions to be observed. **However** it is possible to manipulate certain internal interactions such that the average Hamiltonian is not zero, but something else that we want.

IV. Development of Multiple Quantum Coherence; Use of A Double Quantum Propagator

What do we want as an average Hamiltonian in order to develop multiple quantum coherence? The answer is an average Hamiltonian that allows the density operator at zero time, $\rho(0)$, to evolve in such a manner that $\rho_{1,1\pm k} \neq$ zero· k is the order of the multiple quantum coherence.

The process, then, is to manipulate some internal Hamiltonian with cyclic, periodic rf pulses such that at cycle times nt_c, we have an average Hamiltonian which allows zero-time equilibrium density operator,

$$\rho(0) \equiv \rho_{eq} \sim \sum_i I_{zi}, \qquad i = 1, 2, \ldots$$

containing only diagonal terms representing populations in the Zeeman basis set, to develop multiple quantum coherence, i.e. to develop in such a manner that $\rho_{i,i\pm k} \neq$ zero, for $1 \leq k < \infty$. Since we can only detect single quantum coherence (1Q-COH) with NMR, we note in advance that once produced, the MQ-COH must be reduced to 1Q-COH ***in a manner which reflects the M-Q coherence therein contained*** in order to be detected.

Examples of terms in the density operator which exhibit single quantum coherence might be single spin terms I_i^+ and I_i^-, or two-spin products of the form $I_i^+ I_{z2}$. Double quantum coherence is represented by two-spin product terms in the density operator such as $\sum_{i,j}(I_i^+ I_j^+ + I_i^- I_j^+)$. Triple quantum coherence would be represented by three-spin products such as $I_j^+ I_k^+ I_m^+$.

We can understand how this process works by example. An ensemble of spin 1/2 systems (e.g. protons in solid adamantane) is allowed to come to equilibrium in a static field for a time long compared to T_1. Then

$$\rho(0) \sim \sum_i I_{zi} \tag{20}$$

The sum is over all spins in the sample. Under the influence of an average Hamiltonian, produced by coherent averaging in spin space as discussed for the cases of the spin echo and the dipolar echo, this ensemble is allowed to time-evolve. The formal time evolution formula may be expressed in terms of the product

$$f(A, B) = e^A \cdot B \cdot e^{-A} \tag{21}$$

where A and B are operators.

Fundamental Relation: It may be shown (13) that an equivalent form of this product is

$$e^A \cdot B \cdot e^{-A} = B + [A, B] + [A, [A, B]]/2!$$
$$+[A, [A, [A, B]]]/3! + \ldots$$

i.e.

$$\rho(nt_c) \sim \exp\{-i\bar{H}nt_c\} \cdot \sum_i I_{zi} \cdot \exp\{i\bar{H}nt_c\} \tag{22}$$
$$= \sum I_{zi} + [-int_c\bar{H}, \sum I_{zi}]$$
$$+[-int_c\bar{H}, [-int_c\bar{H}, \sum I_{zi}]]/2! + \ldots \tag{23}$$

The leading term, $\sum_i I_{zi}$ represents populations. The following terms must then be arranged so as to evolve single and higher quantum coherences.

In order to understand how to choose an average Hamiltonian which will produce multiple quantum coherence in the time-developed density operator, $\rho(t)$, as given by eqn. (23), it is necessary to look at the commutation rules for angular momentum operators. We know that

$$[I_{k1}, I_{k2}] = [I_{k1}, I_{k1}] = 0, k = x, y, z$$
$$[I_z, I^\pm] = \pm I^\pm$$
$$[I^\pm, I^+] = \pm 2I_z$$
$$[I^\pm, I^\pm] = 0 \tag{24}$$

Given the form of $\rho_{eq} \equiv \rho(0) \sim \sum_i I_{zi}$, eqns. (22) and (24) immediately tell us that we want $\bar{H}$ to contain terms such as I_i^+. Since we are using the internal homonuclear dipolar coupling Hamiltonian H_{zz} as that which is to be manipulated in order to develop the multiple quantum coherence according to eqn. (25), we realize that we will always be dealing with products between spins 1 and 2 containing terms such as $I_{m1}I_{m2}$, with m = x, y, z.

To begin to think about how rotations in spin space affect the two-body homonuclear dipolar Hamiltonian H_{zz} it is useful to remember (14) that the effect of a rotation of the mth component of angular momentum, I_m, by the operation

$$R_j(\theta)I_m = e^{i\theta I_j} \cdot I_m \cdot e^{-i\theta I_j}$$
$$= I_m\cos(\theta\epsilon_{jmp}) - I_p\sin(\theta\epsilon_{jmp}) \tag{25}$$

where ϵ_{jmp} is zero if any two of j, m, p are the same, unity if j, m, and p represent some cyclic order of x, y, and z, and minus one if the order is anticyclic. Then a result which is found with some algebra is that a rotation of the two-body Hamiltonian for spins 1 and 2, H_{zz}, by ξ about the y axis, followed by a rotation by ϕ about the z yields

$$R_z(\phi)R_y(\xi)H_{zz} = (\omega_D/2)(3\cos^2\xi - 1)H_{zz}$$
$$-(3\omega_D/2)[(I_{z1}I_2^+ + I_1^+I_{z2})e^{-i\phi}]\sin\xi\cos\xi$$
$$+(3\omega_D/2)[I_1^+I_2^+e^{2i\phi} + I_1^-I_2^-e^{-2i\phi}]\sin^2\xi \tag{26}$$

The interesting result shown by eqn. (26) is that a general rotation of H_{zz} in spin space yields a propagator (the exponential of the rotated Hamiltonian) containing populations (H_{zz}), single quantum terms ($I^{\pm_1}I_{z2}$) and double quantum terms ($I_1^{\pm}I_2^{\pm}$). As a special case of this result, we illustrate the formation of a two-quantum propagator under a particularly simple periodic and cyclic sequence (10). This is the sequence (τ, 90_x 4τ, $90_{\bar{x}}$, τ) which we shall denote x, $\bar{x}$. We assume ideal δ function pulses. Under this sequence, the operator $\tilde{I}_z(t)$ is as follows:

$$\begin{aligned} 0 \le t < \tau; \tilde{I}_z &= 1 \cdot I_z = I_z \\ t = \tau; \tilde{I}_z &= R_{90\bar{x}} I_z = -I_y \\ \tau < t < 5\tau; \tilde{I}_z &= -I_y \\ t = 5\tau; \tilde{I}_z &= R_{90\bar{x}} \cdot 1 \cdot R_{90x} I_z = I_z \\ 5\tau < t \le 6\tau; \tilde{I}_z &= I_z \end{aligned} \tag{27}$$

Then, for example, in the time interval $0 \le t < \tau$, $\tilde{H}_{zz} = H_{zz}$ (see eqn. (12)). From an observation of the values of $\tilde{I}_z(t)$, and the recognition that H_{kk} contains the product $\tilde{I}_k\tilde{I}_k$ with k = x, y, z, it is possible to immediately infer the values of $\tilde{H}_{zz}(t)$, and thus to calculate the average Hamiltonian corresponding to H_{zz} to zeroth order:

$$\bar{H}_{zz}^{(0)} = (1/6\tau)\int_0^{6\tau} dt\tilde{H}_{zz} = (1/3)\{H_{zz} + 2H_{yy}\} \tag{28}$$

With the identity $\sum_k H_{kk} = 0$, we find that under the above sequence

$$\bar{H}_{zz}^{(0)} \sim \{-H_{xx} - H_{yy} + 2H_{yy}\} = H_{yy} - H_{xx} \tag{29}$$

The reader will want to verify that under the sequence y, $\bar{y} \equiv (\tau, 90_y, 4\tau, 90\bar{y}, \tau)$ average homonuclear dipolar Hamiltonian is the negative of that found in eqn. (29), i.e. is proportional to $H_{xx} - H_{yy}$. Thus this sequence can be used to produce an average Hamiltonian which will act to reverse, in time, the effect of the average of the average Hamiltonian, $H_{yy} - H_{xx}$, which was used to produce the multiple quantum coherence. As will be seen, this reconversion is performed in such a manner that the information content associated with the multiple quantum coherence is not lost. The means of doing so (*vide infra*) is to phase shift the two-quantum excitation sequence x, $\bar{x}$ with respect to the two-quantum reconversion sequence y, $\bar{y}$ in steps of $2\pi/k_{max}$, where k_{max} is the highest order of MQ-COH to be observed.

With $I^+ = I_x + iI_y$, etc., we find that the average two-body homonuclear dipolar Hamiltonian under the 2-Q excitation sequence x, $\bar{x}$ is proportional to

$$I_1^+I_2^+ + I_1^-I_2^- \tag{30}$$

for the pair of spins $\mathbf{I}_1$, $\mathbf{I}_2$.

Now consider how this sequence can be used to develop multiple quantum coherence for an ensemble of ***pairs*** of dipolar coupled spins I_1 and I_2. We might anticipate in advance that for this simple case, using a two-quantum propagator, all that will be seen are populations, and two quantum coherence. Under this sequence, repeated for n cycle times, $\tau_c = 6\tau$, the time dependence of the density matrix becomes

$$\rho(nt_c) = U_{2Q}\rho(0)U_{2Q}^{-1}$$

where U_{2Q} is, to zeroth order,

$$U_{2Q} = \exp[-(int_c\omega_D/2)\{I_1^+I_2^+ + I_1^-I_2^-\}] \tag{31}$$

Then with $\theta = nt_c\omega_D/2$, eqns. (22), (23) yield

$$\begin{aligned} \rho(nt_c) \sim \{I_{z1} + I_{z2} + i\theta[(I_1^+I_2^+ + I_1^-I_2^-), (I_{z1} + I_{z2})] \\ +(i\theta)^2[(I_1^+I_2^+) + I_1^-I_2^-), [(I_1^+I_2^+ + I_1^-I_2^-), \\ (I_{z1} + I_{z2})]]/2! + \ldots \\ = I_{z1} + I_{z2} - 2i\theta(I_1^+I_2^+ + I_1^-I_2^-) \end{aligned} \tag{32}$$

Only the first two terms in the series represented by eqns. (22) and (23) are non-zero. The remaining terms vanish. Only populations and double quantum coherence remains. At θ near zero, i.e. at times nt_c small compared to the inverse of the dipolar linewidth ω_D^{-1}, there exist only populations. As nt_c becomes of the order of the dipolar linewidth, two-quantum coherence makes its appearance. No more than two-quantum coherence is ever seen regardless of how long the system is allowed to evolve, as one would physically expect from an ensemble consisting of coupled pairs of spins 1/2. The reader will want to verify that for this representation of $\rho(nt_c)$ only the terms $\rho_{11}, \rho_{22}, \rho_{33}, \rho_{13}$, and ρ_{31} are non-zero within the triplet basis set $|I, I_z>$

$$|m> = |3> = |1, 1> = |\alpha\alpha>$$

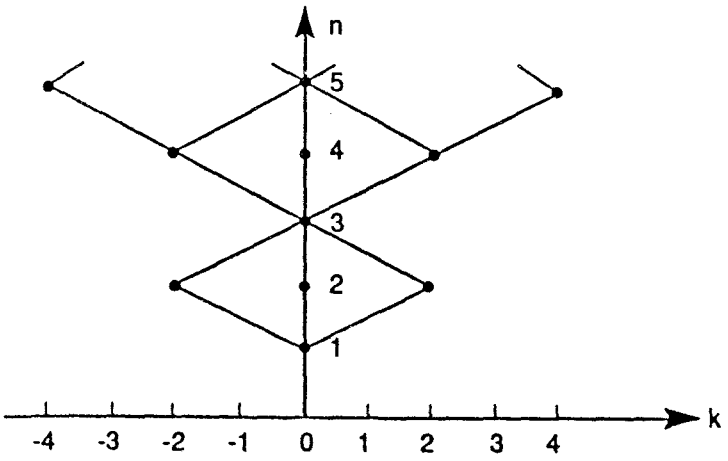

Figure 1: Selection rule for N-spin operator after excitation with a double quantum propagator. The allowed values are k = ±2, ±6, ... for N even and k = 0, ±4, ±8, ... for N odd.

$$|m-1\rangle = |2\rangle = |1,0\rangle = |(\alpha\beta+\beta\alpha)\rangle/\sqrt{2}$$
$$|m-2\rangle = |1\rangle = |1,-1\rangle = |\beta\beta\rangle \qquad (33)$$

by performing the calculations $< m|\rho(nt_c)|m-k>$.

The results just calculated for an ensemble of dipolar coupled spin 1/2 pairs indicate that under the propagator U_{2Q} developed by the sequence $(\tau, 90_x, 4\tau, 90_{\bar{x}}, \tau)$ the selection rules are such that populations and double quantum coherence is observed for an ensemble of pairs of dipolar coupled spins 1/2. More generally, these selection rules for ensembles of n coupled spins may be exhibited by the diagram shown in Figure 1. This diagram states that under this sequence, double quantum coherence will be exhibited by ensembles of 2, 4, 6 ... coupled spins, 4 quantum coherence will be exhibited by ensembles of 5, 7, 9, ... coupled spins, etc.

V. Detection of Multiple Quantum Coherence

We now must consider more closely what was meant by the past statement that the multiple quantum coherence, once produced, must be transferred to 1Q-COH in a manner which reflects the MQ-COH previously produced. As a thought experiment to begin the process, recall the inversion-recovery experiment to measure T_1. In this case, the system is prepared in a state of non-equilibrium populations by an inverting 180° pulse. After a time τ during which the system is allowed to evolve under "T_1 processes", these populations are converted into 1Q-COH using a 90° pulse. The initial intensity of the decay after the "read out" 90° pulse is used, as a function of τ, to calculate T_1. A similar reasoning applies to detecting multiple quantum coherence. The MQ-COH is developed as a function of multiples of the production sequence cycle time t_c. This development is only observable if it is converted into 1Q-COH. During the development, therefore, the MQ-COH is manipulated in such a manner that when converted back into 1Q-COH, the information content of the MQ-COH is contained in the initial intensity of the 1Q-COH which is detected.

To form a picture of how this works, it is useful to think about how the different orders of nQ-COH evolve with time. As indicated in the example in eqn. (32), the higher orders of multiple quantum coherence develop as $\theta \sim nt_c\omega_{Dij}$ increases for the i,jth pair of spins. Therefore, it seems reasonable that the evolution of, e.g. populations, 1Q-COH, and 2Q-COH might look as is shown in Figure 2. I_o represents populations, I_1 the intensity of single quantum coherence, I_2 the intensity of double quantum coherence, etc. Initially one starts with populations. As spin pairs begin to couple to form higher orders of nQ-COH, there is a net loss in populations, and a build up (in the particular example for which the calculation using eqn. (32) was made), first of 2Q-COH, the second term in the expansion of the evolution of ρ, and then of higher orders of MQ-COH as time increases. In the example shown in Figure 2, we assume that we are allowed to build MQ-COH in steps of single quanta, and we will later provide a single quantum propagator U_{1Q} which allows this development to be performed.

Given the development of MQ-COH shown in Figure 2, caused by the single quantum propagator U_{1Q}, it is simple to conceive how one reverses the process to convert back to an observable 1Q-COH. One simply causes the system to evolve under the propagator U_{1Q}^{-1}. Since U_{1Q} will be of the form $\exp\{-i\bar{H}nt_c\}$, with $\bar{H}$ being an average Hamiltonian created by manipulating the homonuclear dipolar interaction, time-reversal is achieved by manipulating the homonuclear dipolar Hamiltonian such that from time nt_c to $2nt_c$ the average Hamiltonian is $-\bar{H}$. In the case of the two quantum propagator, we have seen that the sequence $(\tau/4, 90_x, \tau, 90_{\bar{x}}, \tau/4)$

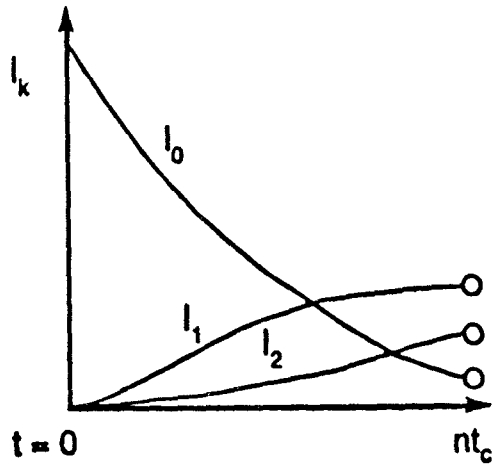

Figure 2: Time evolution of the order of n-Q COH using a single quantum propagator. The intensity of Z-Q COH(I_o) decreases as spin pairs begin to couple to develop the higher order of M-Q COH and build up their intensity(I_1 and I_2).

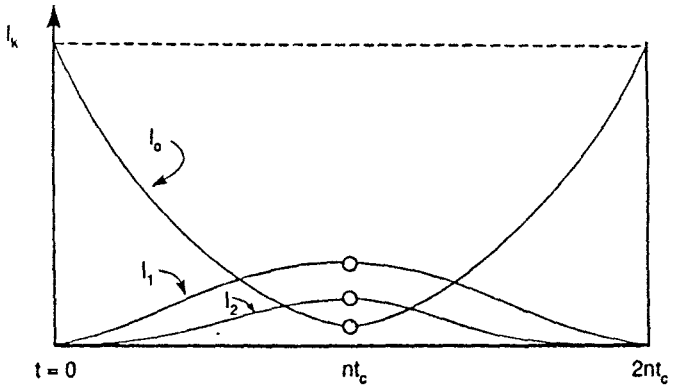

Figure 3: The MQ-COH for higher orders are first created over a time period of nt_c, and then collected this MQ-COH back into Z-Q COH at the time $2nt_c$ by using the negative of the average Hamiltonian. Aside from relaxation, the preparation ($0 \leq t < nt_c$) and mixing period ($nt_c \leq t < 2nt_c$) exactly mirror each other. This diagram illustrates the statement of the cyclic properties of U_{rf}. At the end of $2nt_c$, $I_o(t = 0) = I_o(t = 2nt_c)$.

produces the average Hamiltonian proportional to $H_{yy} - H_{xx}$. We have pointed out that the sequence $(\tau/4, 90_y, \tau, 90_{\bar{y}}, \tau/4)$ results in the average homonuclear dipolar Hamiltonian $H_{xx} - H_{yy} \equiv -(H_{yy} - H_{xx})$. Thus the application of the sequence

$$(\tau/4, 90_x, \tau, 90_{\bar{x}}, \tau/4)n, (\tau/4, 90_y, \tau, 90_{\bar{y}}, \tau/4)n$$

would first create the MQ-COH over a time of n cycle times t_c, and then by time-reversal accomplished by using the negative of the average Hamiltonian during the preparation period, "collect" this MQ-COH back into zero quantum coherence (ZQ-COH) at time $2nt_c$. The process might be visualized as is indicated in Figure 3.

At this point, however, there is no information content in the ZQ-COH shown in Figure 3 at time $2nt_c$ which would be indicative of the MQ-COH created during the times nt_c.

Therefore, as a second thought experiment, dictated by the knowledge that different orders of MQ-COH (***vide infra***) oscillate at multiples of the 1Q-COH under a frequency offset, let us assume that after the production period, nt_c, a frequency offset, δ/Hz, is imposed upon the experiment. Then the behavior of ZQ-COH, 1Q-COH, and 2Q-COH might appear as indicated in Figure 4. The ZQ-COH does not oscillate under an offset. The 1Q-COH will oscillate with period δ^{-1}. The 2Q-COH will oscillate with period $(2\delta)^{-1}$, etc.

Now suppose that the evolution time for MQ-COH under the offset, δ were set to be $(2\delta)^{-1}$. Then at that time, I_1 would be zero, I_o would retain its value at time $t = nt_c$, and I_2 would have oscillated to its value at time $(2\delta)^{-1}$, the period of its oscillation. Therefore, if the reconversion from non-vanishing off-diagonal elements of the density operator back to populations represented by diagonal elements were initiated at time $nt_c + (2\delta)^{-1}$, in the absence of an offset, the value of I_o at time $2nt_c + (2\delta)^{-1}$ would contain ***no contribution*** from the 1Q-COH! The 1Q-COH monitoried as the value of the initial intensity of the FID after a 90° pulse at time $nt_c + (2\delta)^{-1}$ would therefore be lower than that in the absence of an offset. One way of visualizing this result is shown in Figure 5, where different symbols are used to trace the imagined evolution of MQ-COH back into populations after time $nt_c + (2\delta)^{-1}$. The symbol I_n, $n \geq 1$, means the nQ-COH. The symbol I_n^o means the contribution of the nQ-COH developed at time $nt_c + (2\delta)^{-1}$ back into populations. The net magnetization associated with population differences, observed as the initial intensity of the FID after a "read-out" pulse converting population

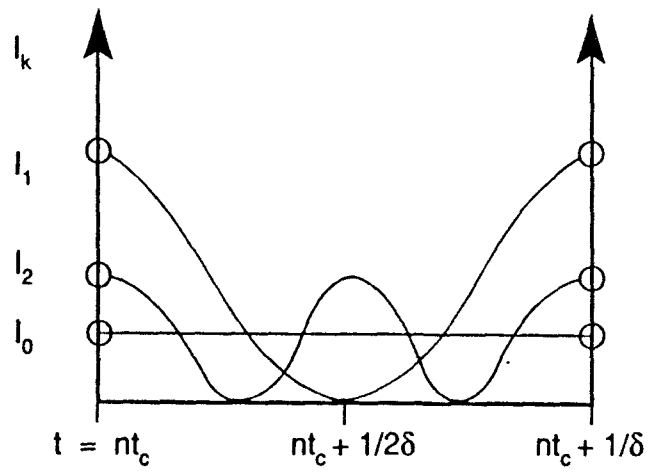

Figure 4: The behavior of Z-Q COH, 1-Q COH and 2-Q COH with a frequency offset, δ/Hz, after the preparation period, nt_c. The n-Q COH has the property of the cosine function, $I_n \infty$ COS(n δ/Hz). See eqn. (39).

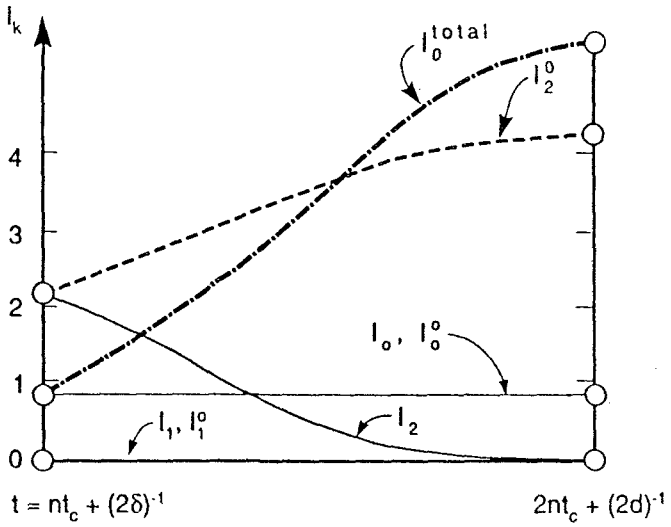

Figure 5: The behavior of the MQ-COH at the evolution time $(2\delta)^{-1}$. I_k^o: the development of Z-Q COH with k-Q COH as its parent.

differences into 1Q-COH, is labeled I_o^{tot}. Clearly, I_o^{tot} will oscillate with time under a frequency offset during the evolution period, and this oscillation provides the means of detecting MQ-COH therein contained, as indicated more analytically below.

The scheme of production, and re-conversion of MQ-COH corresponding to the time development shown in Figure 3, i.e. in the absence of an offset, meaning in the absence of an evolution period, is indicated in Figure 6; a single quantum propagator acts on the ensemble of coupled spins from time zero to time nt_c, and the inverse of that propagator acts for an equal period of time afterwards. The ZQ-COH at time $2nt_c$ is converted into observable 1Q-COH by a 90° "read-out" pulse, and is represented by the initial value of the FID. In the absence of irreversibility, the initial amplitude of the FID detected at time $2nt_c$ will be the same as that detected at time zero after a read out 90° pulse. The equality of these two amplitudes, incidentally, is one means of detecting one's ability to effectively perform time reversal, which is a measure of the perfection of the pulse sequences used.

The imposition of a frequency offset, δ, during the evolution period, to detect MQ-COH at the end of the mixing period, is not without its problems. One is that there is irreversible time evolution of the ensemble during the evolution period due to T_2 processes. A means of avoiding this problem is to realize that imposition of a phase shift (15), ϕ, ***during the preparation period***, $0 \leq t < nt_c$ is formally equivalent to imposition to a frequency offset, and causes the same oscillations of the various orders of MQ-COH as would be observed under a frequency offset. The effect of a phase increment during the preparation period on the detected signal intensity at the end of the mixing period is now considered. In the absence of an evolution period, the initial intensity of the FID detected at the end of the mixing period, $t = 2nt_c$ is

$$< I_z(t = 2nt_c)> = \mathrm{Tr}\{\rho(t = 2nt_c)I_z\} \qquad (34)$$

But

$$\rho(2nt_c) = U_{1Q}^{-1}U_{1Q} \cdot I_z \cdot U_{1Q}^{-1}U_{1Q} = < I_z(t = 0)> \qquad (35)$$

in the absence of irreversibility due to imperfections, and interactions other than homonuclear dipolar coupling. Looking more carefully at the combination of eqns. (34) and (35), and leaving the subscript off the propagators, U, for simplicity, we find that

$$< I_z(t = 2nt_c)> = \mathrm{Tr}\{U^{-1}UI_zU^{-1}UI_z\}$$

$$= \mathrm{Tr}UI_zU^{-1}UI_zU^{-1}$$

$$= \sum_r <r|UI_zU^{-1}UI_zU^{-1}|r>$$

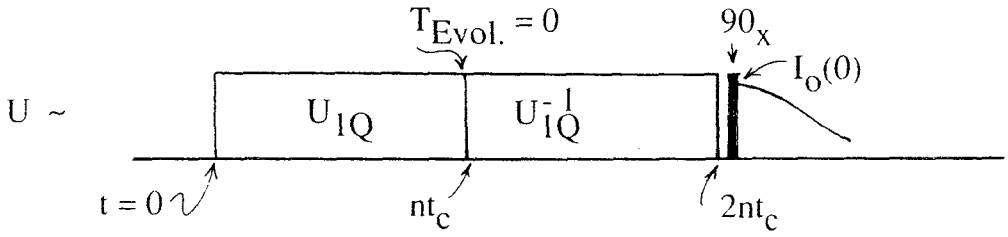

Figure 6: The scheme of 2-D NMR pulse sequence, composed of preparation, evolution, mixing and detection periods, is adapted to develop multiple quantum coherence. The evolution period is set to be zero.

$$= \sum_{r,s} \langle r|UI_zU^{-1}|s\rangle\langle s|UI_zU^{-1}|r\rangle$$

$$= \sum_{r,s} |\langle r|UI_zU^{-1}|s\rangle|^2 \qquad (36)$$

Eqn. (36) has an interesting interpretation. The quantity $U(nt_c,0)I_zU^{-1}(nt_c,0)$ measures how much multiple quantum coherence has been developed under the propagator, U. The quantity $\langle r|UI_zU^{-1}|s\rangle$ measures the k quantum coherence (kQ-COH), where k = r − s, as described earlier, and as will be again illustrated shortly. The term $|\langle r|UI_zU^{-1}|s\rangle|^2$ is the intensity of the kQ-COH. Thus the quantity detected as 1Q-COH by a proper "read-out" pulse at time $t = 2nt_c$ is the result of producing multiple quantum coherence under a propagator, U, acting for a time $t = nt_c$, and converting this coherence back into populations via the inverse propagator U^{-1} during an equal time nt_c.

Now we need to ask "what is the effect of a phase change, ϕ, imposed on ***all*** of the pulses during the preparation period, but not on the pulses during the mixing period, at the total evolution time $t = 2nt_c$?" In this experiment, the "evolution period" identified as the time between the preparation and mixing periods, is zero. A phase change, ϕ, is effected by physically rotating all excitation pulses during the preparation period, by ϕ. This means that a 180_x pulse, for example, becomes $180_{x+\phi}$, and a $180_{\bar{x}}$ pulse becomes a $180_{\bar{x}+\phi}$, etc. The operator form of U rotated by ϕ is just $U\phi = \exp\{-i\phi\}\, I_z \cdot U \cdot \exp\{i\phi I_z\}$. The experimental arrangement is indicated in Figure 7.

The expectation value of I_z detected at times $t = 2nt_c$ will he dependent upon ϕ, as follows:

$$\langle I_z(\phi, 2nt_c)\rangle = \mathrm{Tr}\{U(2nt_c,0)\rho(0)U^{-1}(2nt_c,0)I_z\}$$

$$= \mathrm{Tr}\{U^{-1}_{\phi=0}(2nt_c, nt_c)U_\phi(nt_c,0)I_zU^{-1}_\phi(nt_c,0)$$

$$U_{\phi=0}(2nt_c, nt_c)I_z\}$$

$$\equiv \mathrm{Tr}\{U_o^{-1}U_\phi I_z U_\phi^{-1}U_o I_z\}$$

$$= \sum_{r,s} \langle r|\exp\{-i\phi I_z\}U\exp\{i\phi I_z\}\cdot I_z\cdot\exp\{-i\phi I_z\}$$

$$U^{-1}\exp\{i\phi I_z\}|s\rangle\langle s|UI_zU^{-1}|r\rangle$$

$$= \sum_{k=r-s} e^{-ik\phi}|\langle r|UI_zU^{-1}|s\rangle|^2 \qquad (37)$$

We have noted that the quantity UI_zU^{-1} represents the time development of I_z under the propagator, U, in this case a propagator developing multiple quantum coherence. Non-zero values of $\langle r|UI_zU^{-1}|s\rangle$ indicate non-zero values of r − s = kQ-COH. $|\langle r|UI_zU^{-1}|s\rangle|^2$ is the intensity of the k-Q COH.

The result,

$$\langle I_z(\phi, 2nt_c)\rangle = \sum_{k=-\infty}^{\infty} e^{-ik\phi}|\langle r|UI_zU^{-1}|s\rangle|^2 \qquad (38)$$

may be compared to the value of the free precession decay of a system containing an ensemble of spins oscillating with intensities A_n at frequencies ω_n with some phase ϕ_n with respect to the phase of detection, chosen to be y for the present example;

$$G(t) = \langle I_y(t)\rangle = \sum_n A_n\cos(\omega_n t + \phi_n) \qquad (39)$$

The Fourier transform to the frequency domain reveals the frequency content of G(t), which, with appropriate phase correction, becomes the frequency spectrum; $G(\omega) = F^- G(t)$. By direct analogy, the result eqn. (38) is the superposition in the phase domain, $G(\phi)$, of oscillations with intensities $A_k = |\langle r|UI_zU^{-1}|s\rangle|^2$, and oscillations in the ϕ domain specified by k:

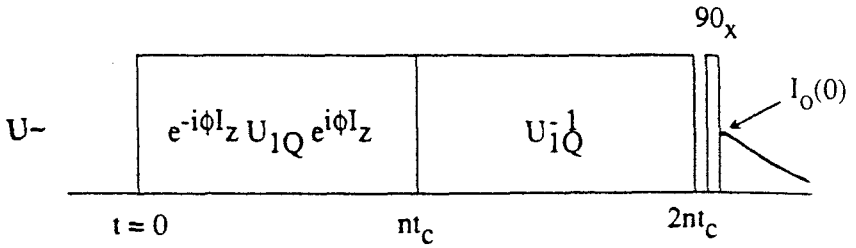

Figure 7: The arrangement of pulse sequence and the way of phase shifting during the MQ experiment is shown. The phases of pulses only in the preparation period are shifted at the same time with the aid of a digital phase shifter, while the phases of the pulses in the mixing period remain unchanged.

$$G(\phi) = \sum_k A_k \cos(k\phi + \delta_k) \qquad (40)$$

The ϕ dependence is experimentally mapped by incrementing the phase of all pulses during the preparation period by $\Delta\phi$, in a series of m experiments at fixed preparation and mixing periods nt_c, and observing the initial value of the FID following a 90° sampling pulse immediately after $t = 2nt_c$. In practice the signal-to-noise ratio is increased if the entire on-resonant decay is integrated from a period after the receiver has recovered from the overload of the 90° pulse until no further signal is present. For strongly dipolar coupled systems with a properly operating solid state spectrometer operating at, say 220 MHz for protons, this means a dead time of about 3 μsec, and an integration period of less than 1 μsec.

The k dependence of $G(\phi)$ is determined from the ϕ Fourier transform. Though it is not obvious from the above discussion, G(f) is symmetric in k, so only the cosine transform is needed;

$$G(k) = (1/\sqrt{2\pi}) \int_o^\infty d\phi G(\phi) \cos k\phi \qquad (41)$$

Therefore, both positive and negative coherences are detected simultaneously. One need use k_{max} phase shifts, $\delta\phi_i$,

$$0 \leq \delta\phi_i \leq \pi \qquad (42)$$

in steps $\Delta\phi = \pi/k_{max}$ to obtain all of the information necessary for the production of a multiple quantum spectrum, G(k), *vs* k, via Fourier transformation of the oscillatory signal, $G(\phi)$, collected from the initial values of the FIDs after the multiple quantum production and collection sequences (i.e. after the preparation and mixing periods). This is to say that to see a multiple quantum spectrum G(k) *vs* k with k extending to k_{max}, one carries out $n = k_{max} + 1$ experiments with phase shifts $\Delta\phi_1 = 0, \Delta\phi_2 = \pi/k_{max}, \Delta\phi_3 = 2\pi/k_{max} \ldots \Delta\phi_n = \pi$. In the absence of irreversibility, the value of $G(\phi)$ *vs* ϕ is symmetric about $\phi = \pi$. Therefore the values of $G(\phi)$ in the range $\pi < \phi \leq 2\pi$ are obtained from the data in the range $0 \leq \phi \leq \pi$. I.e., $G(2\pi) = G(0)$, $G(2\pi - \pi/k_{max}) = G(\pi/k_{max})$, etc. A suitably large number (e.g. 100) of periods of $G(\phi)$ vs ϕ are then stored as an array which can be apodized by the function $e^{-a\phi}$, and Fourier transformed on ϕ to produce the multiple quantum spectrum G(k) *vs* k. This spectrum will show peaks differing by units of 2 quanta each if a two quantum propagator is used or in steps of one quantum each if a single quantum (*vide infra*) is used.

An example of experimental data obtained for $G(\phi)$, with $0 \leq \phi \leq 2\pi$, using a single quantum propagator on adamantane, with phase increments chosen so as to see $k_{max} = 8$ and with 312 μsec of excitation time, is shown in Figure 9. These points repeated 128 times to fit to 2 K size, and tapered by an appropriate apodization function, are shown in Figure 10. The baseline decay represents populations, so it may be subtracted from the oscillations shown in Figure 10 using a baseline adjustment technique before performing the transform on ϕ to yield the multiple quantum spectrum shown in Figure 11. Note that the zero quantum peak is not present in this spectrum.

We now discuss the development of multiple quantum coherence using a single quantum propagator.

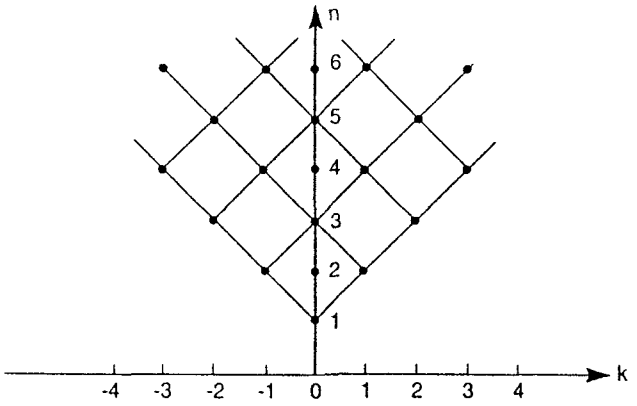

Figure 8: Selection rules for the single quantum propagator used in this work.

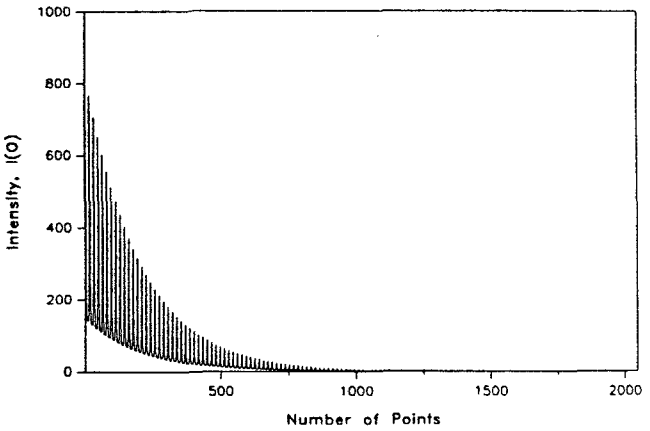

Figure 10: An extension of data point and tapering are performed to generate a data set in the phase domain. Figure 9 was repeated until the number of data points was to 2 K, and then tapered by an appropriate apodization function.

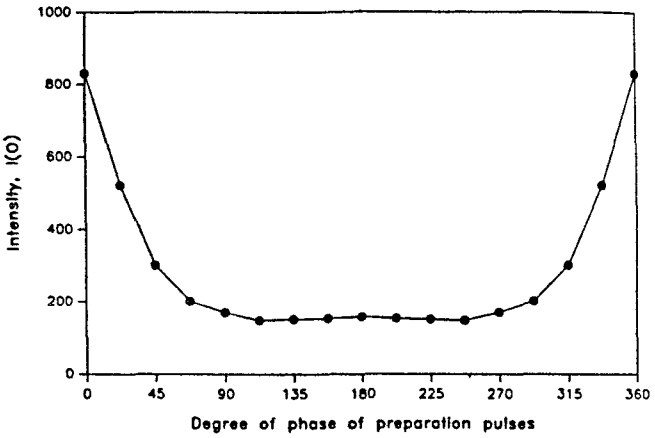

Figure 9: The intensity changes with the phase increment($\Delta\phi$=22.5°) of the preparation pulses are plotted in the phase domain (adamantane). The FID of each phase is transformed to frequency domain, and each point on the plot is obtained by integrating the whole spectrum area, normally from –50 KHz to 50 KHz.

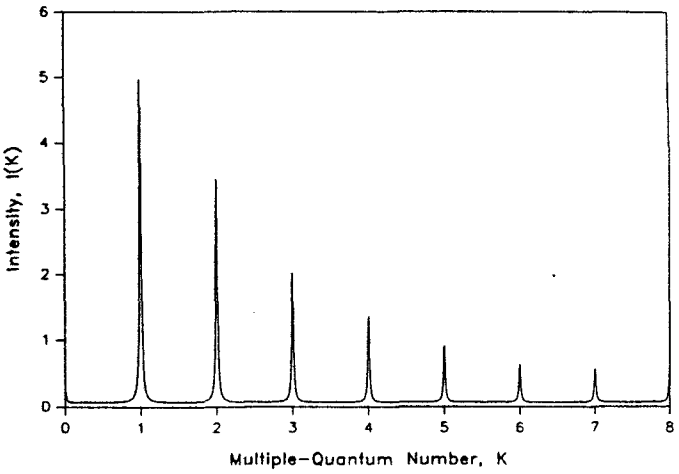

Figure 11: The Fourier transformed spectrum, from phase domain to multiple-quantum number domain. We can see intensity distribution over the multiple-quantum number k=8. The preparation time is 260 μsec. The highest number of quanta, k_{max}, is not seen due to the increment of the phase used.

VI. A Single Quantum Propagator

The development of multiple quantum coherence under pulse sequences resulting in a single quantum propagator for dipolar coupled spin 1/2 systems was first reported and discussed (16) by Suter et al. in 1987. The sequence which we have used to produce the data shown in Figures 9–11 was developed by M. Goldman (17) and essentially identical to that published in 1988 by the Pines' group (18).

This sequence is shown in Figure 12. Important to understanding how this sequence works is an understanding of the development of internal Hamiltonians during finite pulses, an example of which is given in Section V, Chapter 5, of reference 10 for the case of the "flip-flop" phase tuning sequence (τ, 90_x, τ, $90_{\bar{x}}$, τ). Applied to the sequence of Figure 12, the calculation proceeds as follows: consider the time interval $0 \leq t < \tau/4$. Immediately after a perfect δ function rotation by 45°_x at $t = 0$, the value of $\tilde{H}_{zz}$ will be

$$R_x(45^\circ)H_{zz} = (H_{zz} + H_{yy})/2 - 3(I_{z1}I_{y2} + I_{y1}I_{z2})/2 \tag{43}$$

The contribution to $\bar{H}^{(0)}_{zz}$ for this period will then be

$$(1/t_c)\int_0^{\tau/4} \tilde{H}_{zz}dt = (1/t_c)\{(\tau/8)[H_{zz} + H_{yy} - 3(I_{z1}I_{y2} + I_{y1}I_{z2})]\} \tag{44}$$

During the period $\tau/4 \leq t < 5\tau/4$,

$$\begin{aligned}\tilde{H}_{zz}(t) = R_{45x}R_{\xi\bar{y}}H_{zz} = R_{45x}\{&I_1 \bullet I_2 \\ &-3[I_{z1}I_{z2}\cos^2\xi + I_{x1}I_{x2}\sin^2\xi \\ &+(I_{z1}I_{x2} + I_{x1}I_{z2})\sin\xi\cos\xi]\} \\ &= I_1 \bullet I_2 - 3/2\{[z_1z_2 + y_1y_2 \\ &+z_1y_2 + y_1z_2]\cos^2\xi + 2x_1x_2\sin^2\xi \\ &+\sqrt{2}[(z_1 + y_1)x_2 + x_1(z_2 + y_2)]\sin\xi\cos\xi\}\end{aligned} \tag{45}$$

where the symbol z_1z_2 is now used to designate $I_{z1}I_{z2}$, etc., to ease the notation.

During the period $\tau/4 < t < 5\tau/4$, the flip angle ξ varies from zero to 180°. In the interval $\tau/4 < t \leq 5\tau/4$, the contribution of $\tilde{H}_{zz}$ to $H^{(0)}_{zz}$ can be calculated by assuming the flip angle, ξ, to be linear in t, so $\xi = \pi(t-\tau/4)/\tau$, and $dt = \tau\, d\xi/\pi$. Then in the period $\tau/4 \leq t < 5\tau/4$, or $0 \leq \xi < \pi$, the contribution to is $H^{(0)}_{zz}$ is

$$\begin{aligned}\bar{H}_{zz(0)} &= (1/t_c)\int \tilde{H}_{zz}(t)dt \\ &= (1/t_c[\tau\mathbf{I}_1 \bullet \mathbf{I}_2 - 3\{(z_1z_2 + y_1y_2 + z_1y_2 + y_1z_2) \\ &\quad (\tau/2\pi)\int_0^\pi \cos^2\xi d\xi \\ &\quad +x_1x_2(\tau/\pi)\int_0^\pi \sin^2\xi d\xi + [(z_1 + y_1)x_2 + x_1(z_2 + y_2)] \\ &\quad (\tau/\pi\sqrt{2})\int_0^\pi \sin\xi\cos\xi d\xi \\ &= (\tau/2t_c)[(H_{zz} + H_{yy})/2 + H_{xx} - (3/2)(z_1y_2 + y_1z_2)]\end{aligned} \tag{46}$$

In the period immediately following $t = 5\,\tau/4$, and before any other pulses are applied,

$$\tilde{H}_{zz} = 1/2[H_{zz} + H_{yy} - 3(y_1z_2 + z_1y_2)]$$

Proceeding in this manner, it may be verified that the sequence shown in Figure 12, with cycle time $t_c = 6\tau$, yields the following values for the average Hamiltonian associated with the homonuclear dipolar coupling Hamiltonian, H_{zz}, and the chemical shift, $H_{cs} = \sum_{zz} I_z$:

$$\begin{aligned}\bar{H}_{zz} &= -(I_{z1}I_{y2} + I_{y1}I_{z2}) \\ &= -(I_{z1}I_2^+ - I_{z1}I_2^- + I_1^+I_{z2} - I_1^-I_{z2})/2i,\end{aligned} \tag{47}$$

a pure single quantum operator, and $\bar{H}_{cs(0)} = 0$

VII. Applications of Spin Counting With Multiple Quantum Coherence

Applications of multiple-quantum NMR have been extended to various problems in many different areas. The carbon skeleton of organic molecules and proteins in solution can be revealed under the multiple quantum filtering techniques (19, 20), study of liquid crystal conformation (21), and a double quantum propagator has been applied to investigate the arrangement and the size of atoms in solids and liquid crystals (22, 23). In addition, it has been discussed and demonstrated that multiple

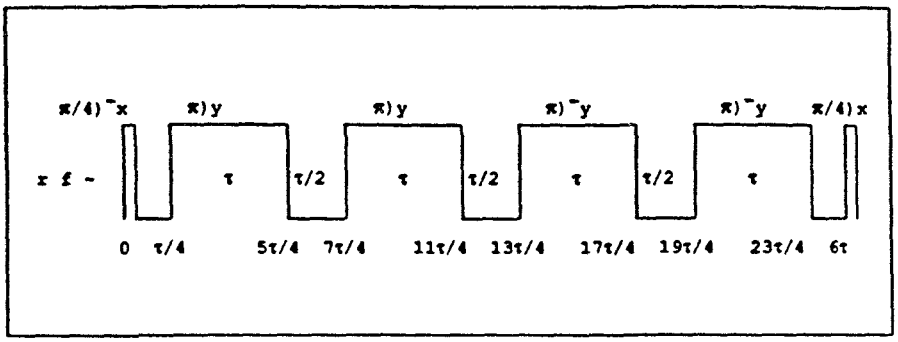

Figure 12: Pulse sequence for the single quantum propagator developed by M. Goldman, and used in this work.

quantum NMR may be applied to the study of relaxation and motion in coupled spin systems (24, 25). By following the development of the highest order of multiple quantum coherence produced as a function of preparation time, Ryoo et al. (26) have studied the distribution of hexamethylbenzene among the cavities of a Na-Y zeolite. The Reimer group (27, 28) used the development of multiple quantum coherence among protons in amorphous silicon hydride and amorphous silicon-carbide-hydride to probe cluster sizes of protons in these systems. In these studies, the development of multiple quantum coherence as a function of development time was used to infer the maximum number of relatively tightly coupled protons. Wang and Slichter (29) used the relative intensities of 1, 2 and 3 quantum coherences to first probe possible identities of C_mH_n fragments resulting from the adsorption and reaction of acetylene on Pt.

The ability to count the number of atoms in a cluster is a powerful tool, when one considers that standard methods of structural characterization, such as x-ray crystallography, can't be applied effectively to the studies of clusters of atoms that occur in materials such as semiconductors, polymers, liquid crystals, zeolites and heterogeneous catalysts.

In order to illustrate some of the principles and techniques used in the above mentioned examples of the use of multiple quantum coherence in spin counting, an example will be given in which the authors have some personal experience. We will consider counting dipolar coupled protons in a hydrocarbon fragment, C_mH_n, deposited on a supported Ru particle (35). In this case, the chemical shift of ^{13}C in the fragments under study was not a unique fingerprint because of the dispersion of chemical environments of the fragments (*vide infra*).

As shown in eqn. (32) and previously discussed (4, 5), the intensities of the various orders of multiple quantum coherence of dipolar coupled spin systems depend on the details of the internuclear distances, and the the excitation time or the cycles of the preparation pulse sequence; Figure 13 shows the MQ-COH spectra of adamantane, obtained under the single quantum propagator discussed in Section 6. In this case, phase increments were chosen such that the highest order of MQ-COH detected was 8. The excitation time ranged from $\tau = 208$ μsec to $\tau = 624$ μsec. Adamantane molecules pack into a face centered cubic solid. Each adamantane molecule is surrounded by 12 nearest neighbors at a distance of 6.60 Å. While intramolecular dipolar interactions are severely attenuated by the rotation of the adamantane molecule in the solid, dipolar interactions between molecules remain, so adamantane represents a system in which there are basically an infinite number of dipolar coupled spins, albeit with dipolar couplings weaker than, e.g. those of protons in crystalline polyethylene. We therefore expect k_{max} to continuously grow as the number of MQ cycles increases. The experimental and theoritical investigation of the time evolution of MQ-COH with the excitation time provides a picture of the many-body interactions which develop the MQ-COH (9, 10, 18, 22, 30–33) and reviewed by Lacelle (34). Shown in Figure 14, to be compared with the result of the thought experiment shown in Figure 2, are the development of multiple quantum coherences of order 1–8, with increase in time over which the coherences can develop. Similar results have been published for hexamethylbenzene (10) and a polycrystalline sample of 1,2,3,4- tetrachloronaphthalene

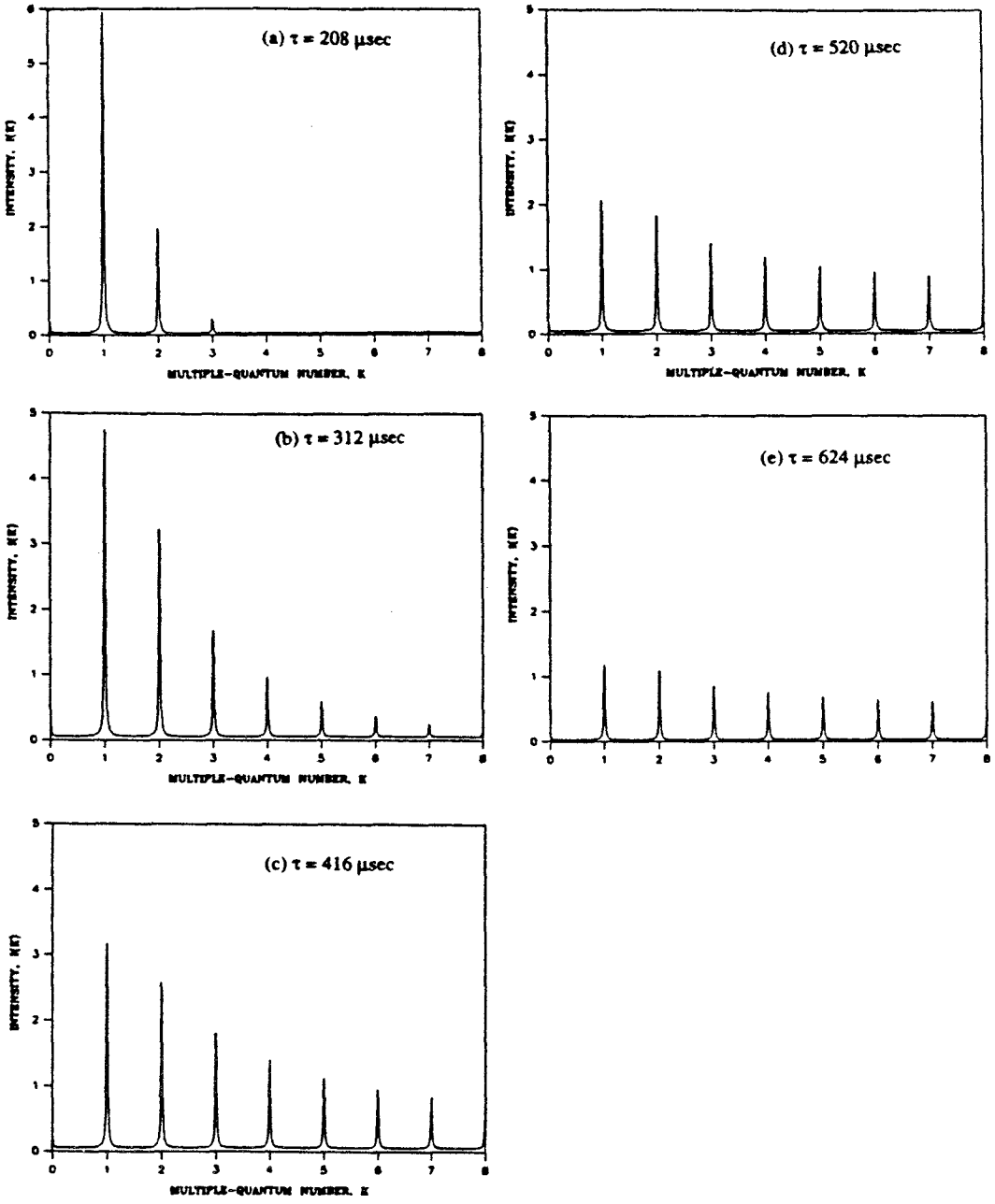

Figure 13: The dependence of Multiple-Quantum spectra of adamantane with various preparation times was recorded. At short preparation times, the number of correlated protons are small: (a) $k_{max} = 3$ for the preparation time, $\tau = 208$ μsec. As the preparation time increases, k_{max} increases so rapidly that it is out of spectral range. Compared to (a), there is not much difference in I(k) after the preparation time of 520 μsec: See (d) and (e).

- bis(hexachlorocyclopentadiene) (22).

As an example of verification that the single quantum propagator discussed above provides multiple quantum coherence in steps of single quanta, a model cluster system lacking long range order can be used, as shown by Baum and Pines (22). The liquid crystal, p-hexyl-p'-cyanobiphenyl in the nematic phase, provides this system. Molecules in a nematic phase are sufficiently mobile to allow the intermolecular dipolar couplings to be averged to zero, while the intramolecular dipolar coupling remain. Since there is no propagation of multiple quantum excitation between the molecules, the liquid crystal in the nematic phase which contains 21 protons is a nice example of a 21-spin cluster. The plot of the k_{max} *vs* the preparation time is given in Figure 15. By the

selection rules for production of multiple quantum coherence under the single quantum propagator and preparation period used in the present experiment (See Figure 8), the number of correlated spins or the number of the atoms in the individual molecules is equal to k_{max} +1. From the trend shown in Figure 15, the limiting value for k_{max} is 20. This value is consistent with the number of protons in the liquid crystal molecule being 21. k_{max} increases as the preparation time increases from zero to 100 μsec. For times greater than 1000 μsec k_{max} keeps remains constant, which confirms that there is no extension of the dipolar coupling network due to translational molecular motion. The multiple quantum spectrum shown in Figure 16, obtained with the phase increment of 5.625° so as to develop a multiple quantum spectrum with k_{max}=32 and with the preparation time of 1092 μsec, indicates that the highest MQ-COH is 20, i.e. $k_{max} = 20$, with negligible intensities after k=20.

With the knowledge that the single quantum propagator discussed in Section 6 does indeed produce multiple quantum spectra in units of single quanta, and that this propagator acting for an excitation time of 310 μsec on the relatively weakly coupled protons in adamantane results in the development of MQ-COH with k > 8, let us now consider the problem of providing possible identifications of C_mH_n fragments strongly adsorbed on supported Ru catalysts reacting with ethylene (35) as a final example of the use of MQ-COH. The reaction of ethylene over Ru/SiO_2 and over $Ru\text{-}Cu/SiO_2$ has been studied by high resolution solid state NMR of ^{13}C (36, 37). It was found that ethylene is transformed to ethane and cis- and trans-2-butene that subsequently hydrogenated to butane. It was also determined that the decomposition of ethylene at room temperature formed adsorbed alkyl groups. However, identification of the rigidly bound intermediates was clouded because they exhibited a very broad ($\sim$ 100 ppm wide) NMR spectrum. Assuming that the strongly adsorbed species formed during the reformation of ethylene were isolated clusters composed of C_mH_n fragments on the surface of catalyst, a single quantum propagator was applied to count the number of protons in the cluster.

The multiple quantum spectrum developed with the preparation time of 312 μsec, which provides $k_{max} = 5$ and 6 protons involved in the C_mH_n fragment, is shown in Figure 17. Experiments with the longer preparation time (up to τ = 572 μsec) confirm that the maximum number of correlated protons in the system under observation is six, for time development less than 600 μsec. Based only on the information that there exist 6 correlated protons, possible strongly bound C_mH_n fragments would be as diverse as (a) neighboring pairs of methyl groups, or (b) neighboring pairs of fragments containing x + y protons, where x + y = 6, (c) one molecule with the actual size of 6 protons and (d) the cluster with 3 protons formed by silanol protons even may be involved in the correlation with C_mH_n to give a 6 proton cluster. However, a simple explanation in accord with the fact that cis- and trans-2-butene are among the observed products is that there is a metallocyclic intermediate such as $Ru\text{-}CH_2\text{-}CH{=}CH\text{-}CH_2\text{-}Ru$ consistent with the results of spin counting. One may also infer that there is not a major contribution from polymeric coke precursors to the rigid species responsible for the observed M-Q coherence. It is assumed that the metallocyclic interrnediate is completely isolated from the other C_mH_n fragments on the multiple quantum time scale.

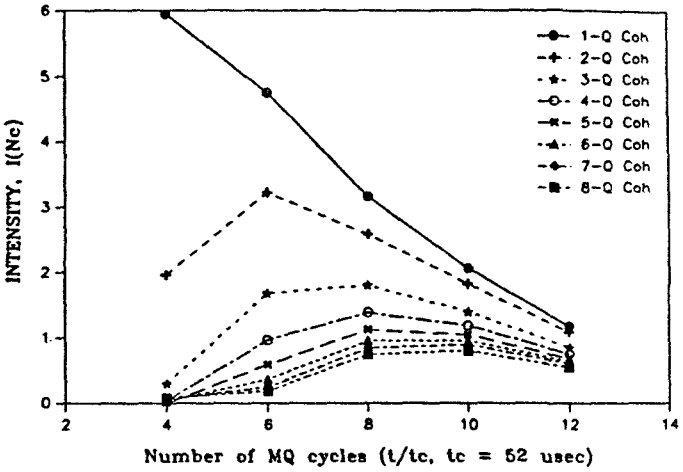

Figure 14: Figure 13 is replotted as a function of the preparation time.

VIII. Acknowledgments

The Ames Laboratory is operated by Iowa State University for the US Department of Energy under contact number W-7405-ENG-82. This work

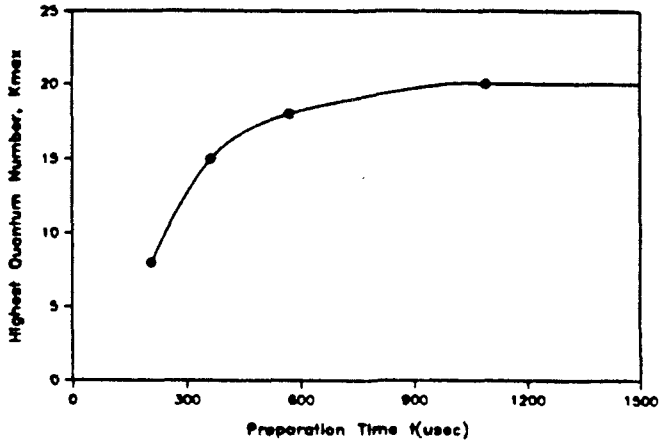

Figure 15: Figure 15. k_{max} vs preparation time for the liquid crystal, p-hexyl-p'-cyanobiphenyl in the nematic phase.

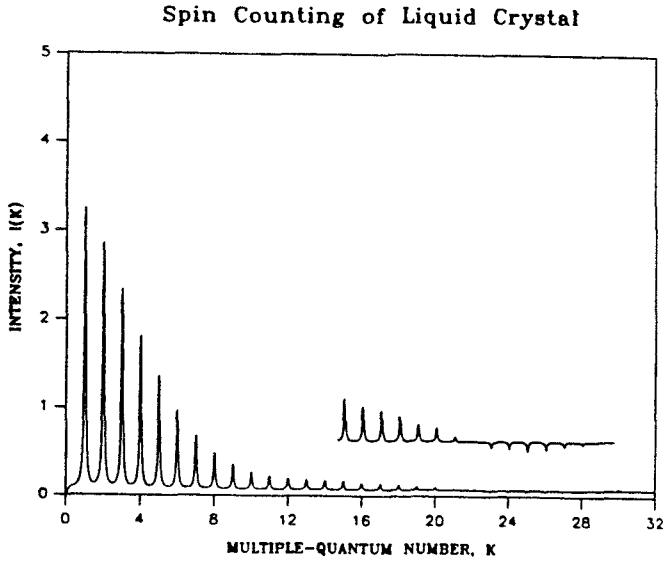

Figure 16: Multiple-quantum NMR spectrum of the liquid crystal, p-hexyl-p'-cyanobiphenyl in the nematic phase (21 coupled protons) with preparation time 1096 μsec. $k_{max} = 20$ shows the full coupling of all spins. The small intensity after k = 20 is noise.

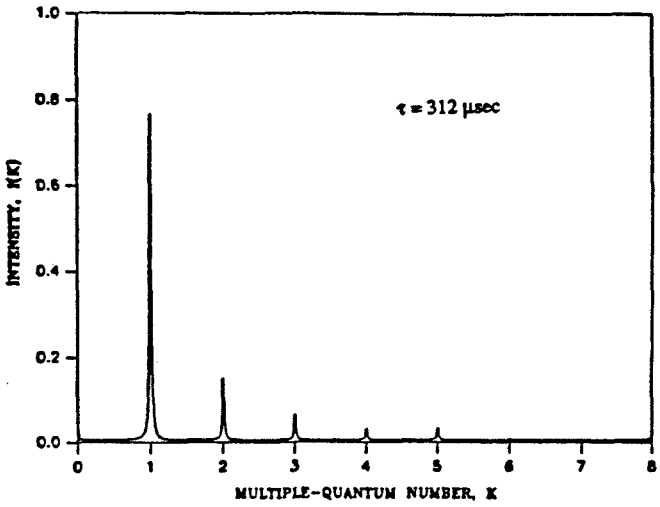

Figure 17: Multiple-quantum spectrum of coupled protons in the strongly bound C_mH_n residue after Ru loaded support was dosed with ethylene, reacted for one hour, pumped at $1x10^{-6}$ Torr for one hour, and sealed. $k_{max} = 5$ indicates a maximum of 6 coupled protons in an isolated C_mH_n fragment. One possibility for the metal-bound fragment is Ru-CH_2- CH=CH-CH_2-Ru.

was supported by the Assistant Secretary for Energy Research, Office of Energy Sciences. WPAS-KC-03-02-01. One of the authors (S. Hwang) wishes to acknowledge the financial support of the Phillips Petroleum Company.

One of the authors (B.C.G.) wishes to express thanks to Maurice Goldman for his patience and instruction during the fall of 1987 in Les Houches, France, and to Wiebren Veeman for his warm hospitality in Nijmegen, The Netherlands the same year, during which a portion of the understanding that led to this review was developed.

IX. References

[1]H. Tanaka, T. Terao, and T. Hashi, *J. Phys. Soc. Japan*, **39**, 378 (1975).

[2]H. Tanaka and T. Hashi, *J. Phys. Soc. Japan*, **39**, 1139 (1974).

[3]W.P. Aue, E. Bertholdi, and R.R. Ernst, *J. Chem. Phys.*, **64**, 2229 (1976).

[4]G. Bodenhausen, *Prog. NMR Spectroscopy*, **14**, 137 (1983).

[5]D. Weitekamp, *Adv. Magn. Res.*, **11**, 111

(1983).

[6]M. Munowitz and A. Pines, ***Adv. Chem. Phys.*** **66**, 1 (1987).

[7]A. Pines, "Lectures on Pulsed NMR" in 100th Fermi School on Physics (Varenna, 1986), B. Maraviglia, ed. North-Holland, 1988.

[8]G. Drobny, ***Ann. Rev. Phys. Chem.***, **26**, 451 (1985).

[9]Y.S. Yen and A. Pines, ***J. Chem. Phys.***, **78**, 3579 (1983).

[10]J. Baum, M. Munowitz, A.N. Garroway, and A. Pines, ***J. Chem. Phys.***, **83**, 2015 (1983).

[11]M. Goldman, (1988) Quantum Description of High Resolution NMR in Liquids, Oxford Press Section 2.5.

[12]B.C. Gerstein and C.R. Dybowski, (1985) Transient Techniques in NMR of Solids; An Introduction to the Theory and Practice, Academic Press, Chapters 4 and 5.

[13]Eqn. (4–19) reference 12.

[14]reference 12, Table 2-1.

[15]S. Emid, ***Physics B***, **128**, 79 (1985).

[16]D. Suter, S.B. Liu, J. Baum, and A. Pines, ***Chemical Physics***, **114**, 103 (1987).

[17]M. Goldman, personal discussions during the RMN summer School organized by J. Virlet in September, 1987, Les Houches, France.

[18]D.N. Shykind, J. Baum, S.-B. Liu, and A. Pines, ***J. Magn. Res.***, **76**, 149 (1988).

[19]M. Munowitz, (1988) Coherence and NMR, Wiley, Chapter 6.

[20]A. Bax, R. Freeman, and T. A. Frenkiel, ***J. Am. Chem. Soc.***, **103**, 2102 (1981).

[21]S.Sinton and A. Pines, ***Chemical Phys. Lett.***, **76**, 263 (1980).

[22]J. Baum and A. Pines, ***J. Am. Chem. Soc.***, **108**, 7447 (1986).

[23]J. Baum, K.K. Gleason, A. Pines, A.N. Garroway, and J.A. Reimer, ***Phys. Rev. Lett.***, **56**, 1377 (1986).

[24]A. Wokaun and R.R. Ernst, ***Molecular Physics***, **36**, 317 (1978).

[25]J. Tang and A. Pines, ***J. Chem. Phys.***, **72**, 3290 (1980).

[26]R. Ryoo, S.-B. Liu, L.C. de Menorval, K. Takegoshi, B. Chemelka, M. Trecoske, and A. Pines, ***J. Phys. Chem.***, **91**, 6575 (1987).

[27]M.A. Petrich, K.K. Gleason, and J. A. Reimer, ***Phys. Rev.***, **B36**, 9722 (1987).

[28]J.A. Reimer and M.A. Petrich, pp 3-27, in "Amorphous Silicon and Related Materials. Ed. Hellmut Fritzsche, World Scientific, (1988).

[29]P-K Wang and C.P. Slichter, ***Phys. Rev. Lett.***, **53**, 82 (1984).

[30]M. Munowitz, A. Pines and M. Mehring, ***J. Chem. Phys.***, **86**, 3172 (1987).

[31]M. Munowitz and M. Mehring, ***Solid State Comm.***, **64**, 605 (1987).

[32]M. Munowitz, ***Molecular Phys.***, **71**, 595 (1990).

[33]W.V. Gerasimowicz, A.N. Garroway, and J.B. Miller, ***J. Am. Chem. Soc.***, **112**, 3726 (1990).

[34]S. Lacelle "On the Growth of Multiple Spin Coherences in the NMR of Solids".

[35]Son-Jong Hwang, T.S. King and B.C. Gerstein, ***Catalysis Letters***, **8**, 367 (1991).

[36]M. Pruski, J.C. Kelzenberg, B.C. Gerstein and T.S. King, ***J. Am. Chem Soc.***, **112**, 4232 (1990).

[37]M. Pruski, J.C. Kelzenberg, M. Sprock, B.C. Gerstein and T.S. King, ***Colloids and Surface***, **45**, 39 (1990).